Sound absorption and dispersion as a function of density near the critical point of xenon*

Jan Thoen† and Carl W. Garland

Department of Chemistry and Center for Materials Science and Engineering, Massachusetts Institute of Technology, Cambridge, Massachusetts 02139

(Received 4 February 1974)

Sound velocity and absorption have been measured at frequencies of 0.6, 1, and 3 MHz for xenon along the liquid-vapor coexistence curve and along several near-critical isotherms. By simultaneously measuring the dielectric constant, the local density was determined at the level in the fluid where the ultrasonic results were obtained. The shape of the coexistence curve obtained from dielectric data gave a critical exponent β of 0.357 ± 0.002. The critical sound absorption and dispersion have been analyzed in terms of our modification of Fixman-Kawasaki theory. It is shown that both absorption and dispersion data can be described in terms of a single reduced frequency. The thermodynamic sound-velocity values needed in the analysis of dispersion have been calculated from the linear-model parametric equation of state.

I. INTRODUCTION

From sonic and ultrasonic investigations information can be obtained about both the thermodynamical and the dynamical behavior of a fluid near a critical point.[1,2] Sound velocities at low enough frequency will be equal to the static adiabatic values. In a one-component fluid, the relation between this limiting adiabatic velocity $u(0)$ and other thermodynamic quantities is given by

$$u^2(0) = \frac{1}{\rho\kappa_S} = \frac{1}{\rho\kappa_T} + \frac{T(\partial P/\partial T)_v^2}{\rho^2 C_v}, \tag{1}$$

where κ_S and κ_T are, respectively, the adiabatic and isothermal compressibilities, ρ is the mass density, and C_v is the specific heat at constant volume. Near the critical point both κ_T and C_v diverge; however, κ_T has a strong singularity while C_v diverges quite weakly. As a consequence, close to the critical point the contribution of the first term on the right-hand side of Eq. (1) is negligible compared to the second term. Thus the behavior of $u(0)$ near the critical point will be almost completely determined by the character of the C_v singularity since the other quantities in the second term are constant or slowly varying. It follows that low-frequency sound-velocity measurements allow one to study the specific-heat singularity[3,4]; in particular, see the following article[5] for a 1-kHz investigation of xenon.

On the other hand measurements of the sound velocity $u(\omega)$ and the amplitude attenuation per wavelength $\alpha_\lambda(\omega)$ as a function of frequency provide important information about the dynamical aspects of structural relaxation processes near a critical point.[6,7] The present investigation was designed to extend and clarify the experimental data characterizing the dynamical behavior in the critical region of xenon. A previous ultrasonic study of xenon[8] in the 0.4–5-MHz range involved measuring the temperature dependence of $u(\omega)$ and $\alpha_\lambda(\omega)$ for a mean filling density of $1.01\rho_c$ and the pressure dependence of $u(\omega)$ and $\alpha_\lambda(\omega)$ along several isotherms. The pressure is both experimentally and theoretically an awkward independent variable for characterizing isothermal measurements near T_c. More importantly, gravity-induced density gradients gave rise to large uncertainties in the local density as a function of height in the cell.

In this paper we report on an ultrasonic experiment in which these difficulties were avoided. The local density in the fluid at the level of the ultrasonic measurements could be obtained by simultaneously measuring the dielectric constant as a function of height with an array of narrow capacitors located close to the acoustical path. As a result, our ultrasonic data were obtained at well-specified densities and could be analyzed directly as a function of the order parameter $\rho-\rho_c$. The previously reported behavior along the critical isochore[7,8] is confirmed, and the critical dynamical behavior is established along the coexistence curve and along near-critical isotherms.

II. EXPERIMENTAL METHOD

In order to make accurate measurements of both sound velocity and absorption close to the critical point, a phase-sensitive detection scheme which incorporates signal averaging was used in a variable-path-length interferometer. Accurate measurements could be made with this method even when the attenuation was as large as 0.4 Np per wavelength (a typical value close to the critical point). A complete description of this acoustic technique has been given elsewhere.[9] Detailed information about the ultrasonic interferometer, the

measuring cell, and the temperature controlling system can also be found elsewhere.[8,10] However, two modifications were made for the present work. The temperature was measured with a Leeds and Northrup model 8164-B calibrated platinum resistance thermometer instead of the previously used quartz thermometer, for which large zero-point shifts had been observed.[8] In addition an array of 15 narrow-strip capacitors was mounted inside the cell close to the acoustical path.

The capacitor array shown in Fig. 1 was obtained by gold-plating horizontal strips on two vertical plates of very-low-thermal-expansion glass (Corning ULE-7971). The total height of both glass pieces was 1.750 in. Twelve of the strips on the left-hand piece in Fig. 1 were 0.0625 in. high, two were 0.125 in. high, and one (at the top) was 0.250 in. high. The two glass pieces were separated by four 0.005-in.-thick spacers made of the same glass. The different pieces were clamped together on an Invar steel supporting block (not shown) using small bolts and spring washers. The edges and the back of the glass pieces were also gold plated

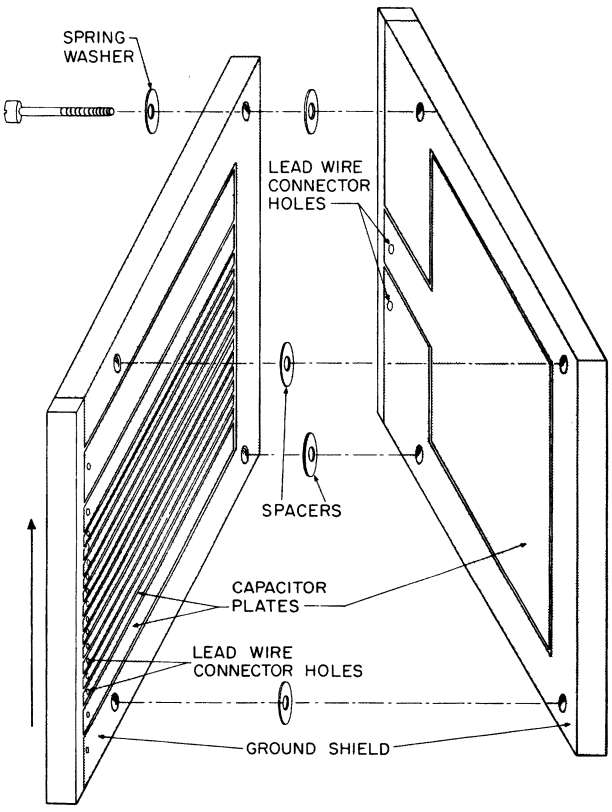

FIG. 1. Detailed view of the capacitor array. The arrow indicates both the vertical direction in the cell and the direction of acoustic propagation.

to provide the necessary shielding between the actual capacitor plates and the lead wires. Measurements were made at different levels in the cell by using the large (almost square) strip on the right-hand piece in Fig. 1 as one capacitor plate and picking out one of the small strips as the other plate of the capacitor. All other strips on the left-hand piece were connected to the shield potential. By externally interchanging lead wires, 15 readings of the dielectric constant were obtained at different well-defined heights in the cell. The dielectric constant was readily obtained from the ratio of the capacitance value C obtained in the fluid and its value C_0 measured in vacuum. The capacitance readings were obtained with a General Radio 1615-A bridge. The vertical position of the ultrasonic transducers with respect to the capacitor strips could be accurately determined.

III. EXPERIMENTAL RESULTS

Sound velocity and absorption have been measured at frequencies of 0.6, 1, and 3 MHz. Extensive data were obtained in both the coexisting liquid and vapor phases between 14°C and the critical temperature (16.643°C), along three supercritical isotherms (16.669, 16.803, and 17.031°C), and along one subcritical isotherm (16.507°C). Additional 1-MHz velocity data were also obtained over an extended temperature range between 5 and 14°C in both coexisting phases. For each of the ultrasonic data points the corresponding value for the local density was obtained by measuring the dielectric constant.

The dielectric-constant values can be converted to densities using the Clausius-Mosotti relation

$$E \equiv \frac{\epsilon' - 1}{\epsilon' + 2} = \tfrac{4}{3}\pi\alpha'\rho \equiv K_1\rho\,, \tag{2}$$

where ϵ' is the dielectric constant and α' is the molecular polarizability of the fluid. In the analysis of the ϵ' data we have assumed that for the small temperature and relatively small density range of our investigation α' had a constant value. It has been experimentally shown that this is a good approximation.[11,12] For temperatures below T_c it was possible to measure the dielectric constant ϵ' in both coexisting phases by adjusting the amount of xenon in the cell in such a way that not all 15 capacitors were in the same phase. Results for the quantity E along the coexistence curve were least-squares fitted with the following power-law expression:

$$E_L - E_V = K_1(\rho_L - \rho_V) = K_2\left(\frac{T_c - T}{T_c}\right)^{\beta}, \tag{3}$$

in which K_2, T_c, and β were adjustable parameters.

The uncertainty in T_c arising from fitting the data with Eq. (3) was less than 0.001°C. The best fit (shown in Fig. 2) was obtained for $T_c = 16.643$°C and gave $K_2 = 0.320 \pm 0.002$ and $\beta = 0.357 \pm 0.002$. From an analysis of the rectilinear diameters a value for $E_c = K_1 \rho_c$ could also be derived. This allowed us to convert all experimentally obtained values of E into reduced densities Δ since

$$\Delta \equiv (\rho - \rho_c)/\rho_c = (E - E_c)/E_c . \tag{4}$$

Both the amplitude absorption per wavelength $\alpha_\lambda(\omega)$ and the sound velocity $u(\omega)$ for 0.6, 1, and 3 MHz are given in Fig. 3 as a function of the reduced density along the three supercritical isotherms. The data obtained in the coexisting phases are displayed in Fig. 4. A very large critical absorption and velocity dispersion are obvious in these two figures. Table I gives the numerical values for the data shown in Figs. 3 and 4. Table II contains 1-MHz velocity data in both coexisting phases for the extended temperature range between 5.5 and 14.4°C.

All the 1-MHz results near the critical point are shown together in Fig. 5. From this figure it can easily be seen that u(1 MHz) has a well-defined finite value at the critical point. Similar figures can be obtained for the results at 3 and 0.6 MHz with the important difference that the minimum values observed for $u(\omega)$ are respectively higher (about 7 m sec^{-1}) or lower (about 2.5 m sec^{-1}) than the 1-MHz value. It is worth noting that the minimum in $u(\omega)$ and the maximum in $\alpha_\lambda(\omega)$ occur at $\rho = \rho_c$ along all three supercritical isotherms. The temperature variations of these values along the critical isochore are completely consistent with our choice of T_c based on the analysis of coexisting densities. Thus, there is no indication of a difference between T_c and $T_{\min}$, the temperature of the velocity minimum along the critical isochore (see Ref. 8).

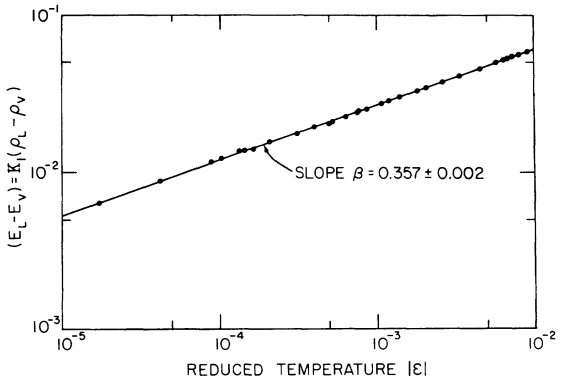

FIG. 2. Power-law fit to the coexistence curve of xenon near its critical point. The line represents a least-squares fit of Eq. (3) to the experimental points with $T_c = 16.643$°C, $\beta = 0.357 \pm 0.002$, and $K_2 = 0.320 \pm 0.002$.

IV. PARAMETRIC EQUATION OF STATE

Even for a well-studied system like xenon direct experimental results for several thermodynamic properties are not available near the critical point, especially along the coexistence curve and along near-critical isotherms. In particular, $u(0)$ and C_v are important quantities whose values are needed in the analysis of the dynamical behavior (see Sec. V). Thus we shall resort to a calculation of such properties from the "linear-model" parametric equation of state.

A very convenient equation of state near the critical point has been proposed by Schofield, Litster, and Ho.[13] This equation of state is based on the parametric representation of scaling laws.[14,15] The equation is given in terms of the parametric variables r and θ, where r is essentially the radial distance from the critical point and θ describes the angular position in the (ρ, T) plane. These parametric variables are defined by

$$\frac{\mu(\rho, T) - \mu_0(\rho_c, T)}{P_c/\rho_c} \equiv \Delta\mu = a\theta(1 - \theta^2) r^{\beta\delta} , \tag{5}$$

$$(T - T_c)/T_c \equiv \epsilon = (1 - b^2\theta^2) r , \tag{6}$$

where $b > 1$ and β and δ are the usual critical exponents. The constants a and b have to be determined from experimental data. The parametric equation of state can then be written in the fo'lowing general form:

$$(\rho - \rho_c)/\rho_c \equiv \Delta = \mathfrak{K}(\theta) r^\beta . \tag{7}$$

For the unknown polynomial $\mathfrak{K}(\theta)$ Schofield, Litster, and Ho introduced the "linear-model" ansatz

$$\Delta = k\theta r^\beta , \tag{8}$$

where k is a positive constant that must be determined from experimental data. One of the great advantages of this equation of state is that by using the relation

$$\mu = \left(\frac{\partial A}{\partial \rho}\right)_T \tag{9}$$

for the chemical potential per gram, one is able to integrate Eq. (5) to find the free energy per unit volume $A(\rho, T)$ and arrive at closed-form expressions for all the thermodynamic functions. It can readily be seen from Eqs. (5)–(8) that the critical isotherm ($\epsilon = 0$) is given by $\theta^2 = b^{-2}$, with $\theta \gtrless 0$ for $\rho \gtrless \rho_c$ and $\theta < 0$ for $\rho < \rho_c$. The critical isochore for $\epsilon > 0$ is given by $\theta = 0$, the coexisting liquid by $\theta = 1$,

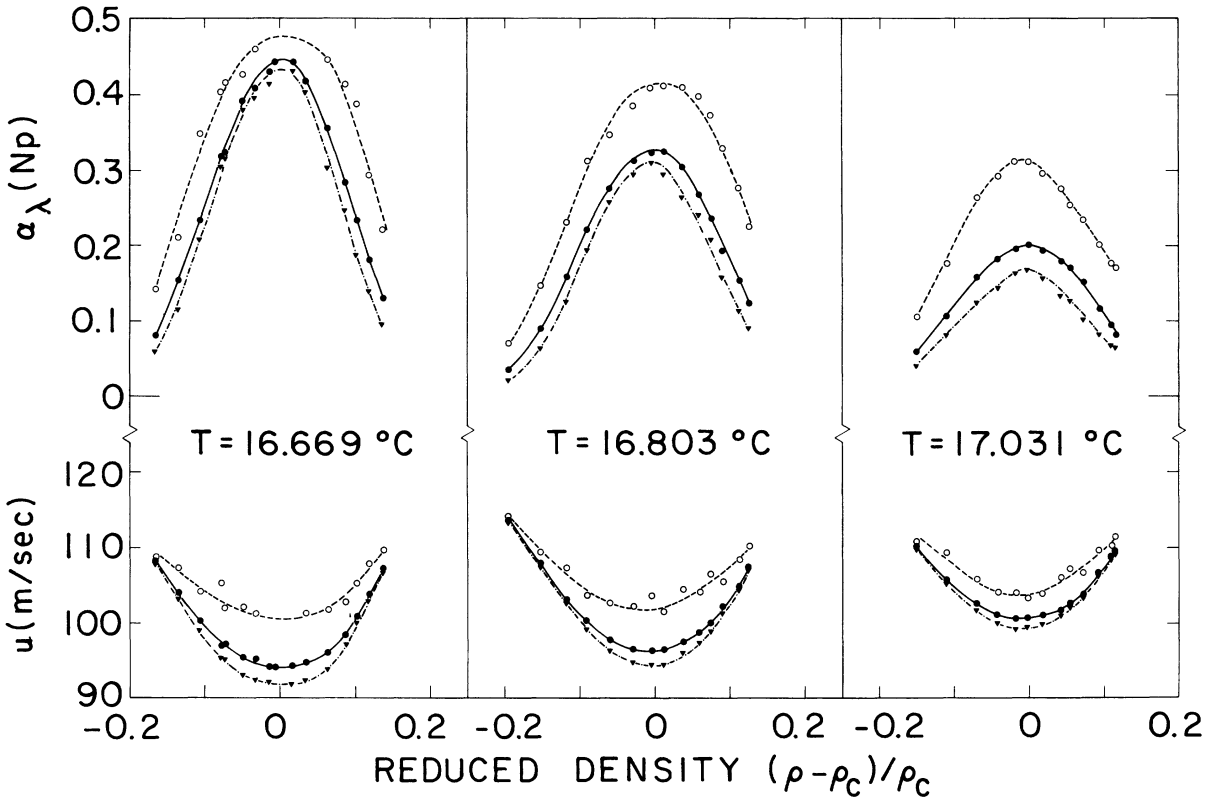

FIG. 3. Sound velocity $u(\omega)$ and the absorption per wavelength $\alpha_\lambda(\omega)$ as a function of reduced density along three supercritical isotherms. Open circles, 3 MHz; solid dots, 1 MHz; and inverted triangles, 0.6 MHz.

and the coexisting vapor by $\theta=-1$. Recently Hohenberg and Barmatz[16] (HB) used the linear model for the study of gravity effects near the gas-liquid critical point and derived expressions for several thermodynamic properties. A detailed discussion of the linear model has been given by HB and a more general discussion of parametric equations of state by Fisher.[17] *The dimensionless units for the different thermodynamic properties defined by* HB *are used in the present paper.*[18]

The determination of the linear-model parameters proceeds as follows. The parameters a and k in Eqs. (5) and (8) can be obtained from the shape of the coexistence curve,

$$(\rho_L-\rho_c)/\rho_c \equiv \Delta_L(\epsilon) = B(-\epsilon)^\beta , \tag{10}$$

and from compressibility data for $\rho=\rho_c$ and $\epsilon>0$,

$$\kappa_T = \Gamma\epsilon^{-\gamma} . \tag{11}$$

The parameter b is usually derived from the shape of the critical isotherm,

$$\Delta\mu = D\Delta|\Delta|^{\delta-1} , \tag{12}$$

or from the ratio of the prefactors Γ/Γ', with Γ given by Eq. (11) and Γ' defined by the power-law expression for the isothermal compressibility in the coexisting phases (using the linear model result $\gamma'=\gamma$),

$$\rho^2\kappa_T = \Gamma'(-\epsilon)^{-\gamma} . \tag{13}$$

This leads to the following relations (see HB) for the parameters:

$$D = ab^{\delta-3}k^{-\delta}(b^2-1) , \tag{14}$$

$$\Gamma/\Gamma' = 2(b^2-1)^{1-\gamma}/[1-b^2(1-2\beta)] . \tag{15}$$

As pointed out by HB the uncertainties in the experimental values of D, B, Γ, and Γ' lead to a range of b^2 values so that for practical purposes one chooses b^2 by the "minimization" condition proposed in Ref. 13:

$$b^2 = (\delta-3)/(\delta-1)(1-2\beta) . \tag{16}$$

The value for b^2 obtained in this way falls within the range of b^2 values derived from presently available experimental data for D, B, Γ, and Γ'. Expression (16) also gives rise to simplifications in the thermodynamic functions. On integrating Eq. (5) using relation (9), one arrives at the following result for the free energy:

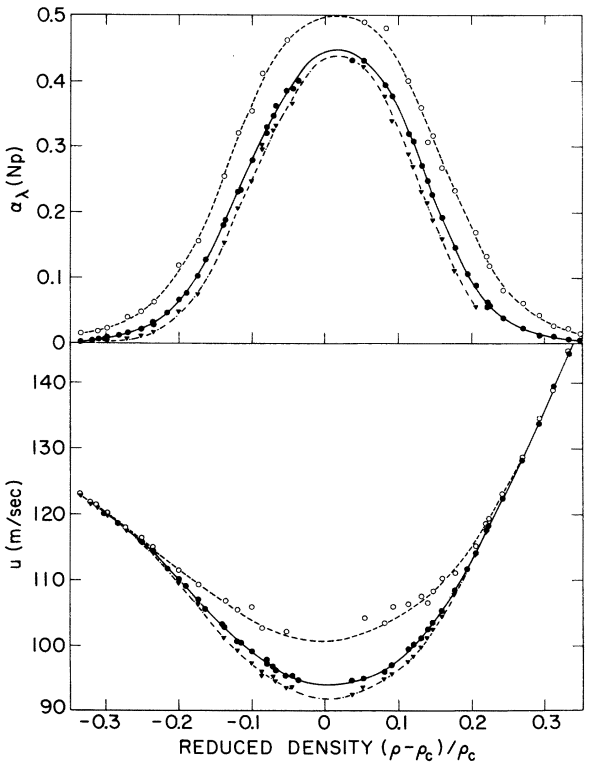

FIG. 4. Sound velocity $u(\omega)$ and the absorption per wavelength $\alpha_\lambda(\omega)$ as a function of reduced density along the coexistence curve. Open circles, 3 MHz; solid dots, 1 MHz; and inverted triangles, 0.6 MHz.

$$A(\rho, T) = A_s(\rho, T) + \mu_0(\rho_c, T)\rho + A_0(T), \quad (17)$$

where $A_s(\rho, T)$ is the singular part given in terms of r and θ by HB and where $\mu_0(\rho_c, T)$ and $A_0(T)$ are assumed to be analytic functions of T near T_c. Thus we can write the following power-series expansions:

$$A_0(T) = A_0(T_c) + A_0'(T_c)\epsilon + A_0''(T_c)\tfrac{1}{2}\epsilon^2 + A_0'''(T_c)\tfrac{1}{6}\epsilon^3 + A_0''''(T_c)\tfrac{1}{24}\epsilon^4 + \cdots, \quad (18)$$

$$\mu_0(T) = \mu_0(T_c) + \mu_0'(T_c)\epsilon + \mu_0''(T_c)\tfrac{1}{2}\epsilon^2 + \mu_0'''(T_c)\tfrac{1}{6}\epsilon^3 + \mu_0''''(T_c)\tfrac{1}{24}\epsilon^4 + \cdots. \quad (19)$$

Values for the coefficients in these equations have to be obtained from experimental results. HB retained the constants A_0', A_0'', and μ_0''. The quantity $(A_0'' + \rho\mu_0'')$ is then the "background" specific heat along the critical isochore, and μ_0'' is obtained from the asymmetry of C_v about $\rho = \rho_c$ on an isotherm far above T_c. The slope of the critical isochore $(\partial P/\partial T)_{\rho_c}$ at T_c determines the value of the constant A_0'. HB derived the appropriate constants for several fluids so that one can readily calculate numerical values for any given thermodynamic quantity.[19] Using the values for the xenon parameters quoted by HB we calculated the zero-frequency sound velocity for the range of our experimental results. The reliability of these calculated results could be tested outside the dispersion region ($\omega^* < 0.1$; see Sec. V) by comparison with our experimental megahertz results and the low-frequency (kilohertz) results along the critical isochore.[4,5] The over-all agreement was rather poor, especially along the coexistence curve. It seems likely that the form $(A_0'' + \rho\mu_0'')$ introduced by HB for the background term in the specific heat C_v is inadequate. At least, changing the numerical values of A_0'' and μ_0'' did not give any substantial improvement.

Since we are primarily interested in a good prediction of the zero-frequency sound velocity near T_c, we decided to derive the parameters of the linear model from a least-squares fit of the available kilohertz and megahertz results outside the dispersion region (mainly results for $\rho = \rho_c$ and magahertz results for both coexisting phases). At

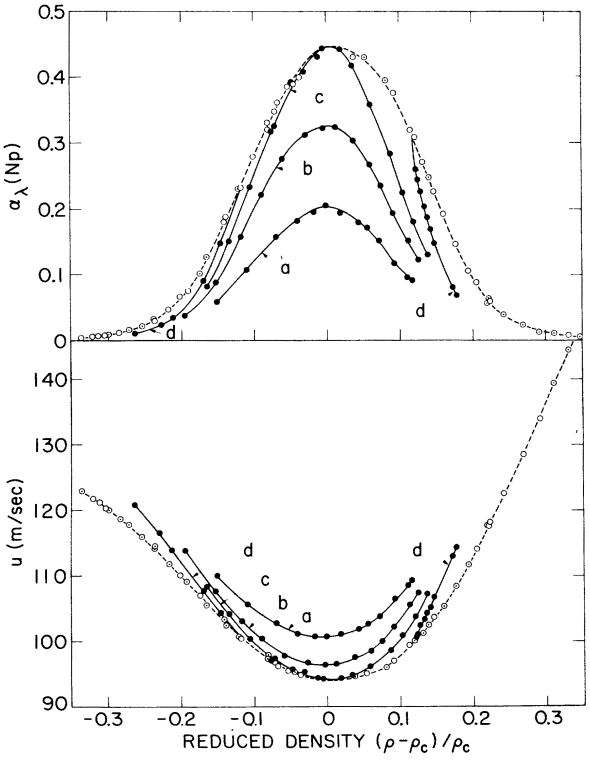

FIG. 5. Sound velocity and absorption in xenon at a frequency of 1 MHz as a function of the reduced density. The dashed line and open circles represent results in the coexisting liquid and vapor phases. Curves *a*, *b*, and *c* are supercritical isotherms at 17.031, 16.803, and 16.669°C, respectively. Curve *d* is a subcritical isotherm at 16.507°C.

TABLE I. Sound velocity and attenuation per wavelength (at 0.6, 1, and 3 MHz) along three supercritical isotherms and in the coexisting liquid and vapor phases.

T (°C)	$\Delta\rho/\rho_c$	u (m/sec)			α_λ (Np)			T (°C)	$\Delta\rho/\rho_c$	u (m/sec)			α_λ (Np)		
		0.6	1	3	0.6	1	3			0.6	1	3	0.6	1	3
17.031	0.1163	109.4	109.3	111.3	0.0637	0.0907	0.170	16.803	−0.0601	96.3	97.7	102.7	0.256	0.275	0.346
	0.1100	108.5	108.5	110.2	0.0665	0.0955	0.176		−0.0904	99.2	100.4	103.7	0.193	0.220	0.312
	0.0921	106.1	106.5	109.6	0.0812	0.116	0.201		−0.1181	102.7	103.0	107.3	0.123	0.157	0.230
	0.0723	103.3	103.7	106.7	0.101	0.151	0.234		−0.1523	107.5	107.7	109.3	0.0620	0.0882	0.145
	0.0552	102.0	102.7	107.2	0.126	0.170	0.253		−0.1950	113.6	113.7	113.9	0.0204	0.0347	0.0693
	0.0431	101.1	101.7	106.0	0.132	0.178	0.275								
	0.0177	99.8	101.1	103.9	0.155	0.193	0.295	16.669	0.1372	106.8	107.2	109.6	0.0951	0.130	0.220
	−0.0015	99.4	100.7	103.4	0.166	0.205	0.310		0.1188	103.3	103.8	107.8	0.139	0.180	0.293
	−0.0179	99.2	100.6	104.0	0.162	0.194	0.311		0.1025	100.0	100.9	105.2	0.186	0.233	0.387
	−0.0414	100.1	101.0	105.1	0.142	0.181	0.292		0.0874	97.1	98.5	102.9	0.246	0.283	0.413
	−0.0699	101.7	102.7	105.8	0.123	0.157	0.263		0.0637	93.8	96.1	101.8	0.303	0.358	0.445
	−0.1103	105.4	105.5	109.3	0.0799	0.106	0.175		0.0345	92.4	94.8	101.4	0.400	0.417	•••
	−0.1506	109.9	110.0	110.7	0.0393	0.0586	0.105		0.0180	91.9	94.4	•••	0.432	0.442	•••
									−0.0063	•••	94.1	•••	•••	0.443	•••
16.803	0.1247	106.9	107.3	110.1	0.0877	0.122	0.224		−0.0131	92.2	94.2	•••	0.414	0.430	•••
	0.1119	104.4	104.6	108.4	0.111	0.152	0.275		−0.0317	92.5	95.3	101.3	0.395	0.408	0.460
	0.0899	101.3	102.2	105.5	0.156	0.192	0.328		−0.0488	93.2	95.5	102.1	0.380	0.392	0.426
	0.0745	98.8	100.0	106.5	0.206	0.235	0.373		−0.0725	95.2	97.3	102.0	0.316	0.324	0.416
	0.0587	97.3	98.4	104.1	0.239	0.267	0.397		−0.0780	95.4	97.0	105.3	0.305	0.318	0.403
	0.0368	96.0	97.5	104.4	0.261	0.303	0.409		−0.1060	99.0	100.3	104.2	0.208	0.233	0.349
	0.0115	94.4	96.5	101.5	0.293	0.324	0.410		−0.1352	103.3	104.1	107.3	0.117	0.154	0.210
	−0.0044	94.5	96.4	103.6	0.308	0.322	0.408		−0.1645	108.0	108.3	108.6	0.0598	0.0813	0.141
	−0.0285	94.8	96.7	102.3	0.293	0.312	0.384								
			Coexisting liquid								Coexisting vapor				
16.638	0.0361	92.5	94.7	•••	•••	0.430	•••	16.638	−0.0375	•••	94.8	•••	•••	0.399	•••
16.631	0.0511	93.6	95.0	104.2	0.420	0.430	0.489	16.636	−0.0514	93.6	95.3	•••	0.365	0.388	•••
16.602	0.0805	94.9	96.0	103.5	0.376	0.394	0.480	16.629	−0.0537	93.5	95.5	102.2	•••	0.385	0.462
16.584	0.0906	95.6	97.0	106.0	0.338	0.376	•••	16.618	−0.0689	94.5	96.2	•••	0.331	0.362	•••
16.529	0.1128	97.5	99.5	106.3	0.287	0.319	0.399	16.614	−0.0714	95.1	96.8	•••	0.325	0.347	•••
16.500	0.1197	98.3	100.2	•••	0.268	0.308	•••	16.605	−0.0806	95.3	97.4	•••	0.296	0.330	•••
16.464	0.1313	99.7	101.2	107.5	0.231	0.270	0.359	16.596	−0.0812	95.9	97.9	102.7	0.302	0.320	0.412
16.428	0.1394	101.1	102.5	106.5	0.213	0.247	0.307	16.554	−0.1014	97.2	99.1	105.8	0.246	0.278	0.353
16.402	0.1460	102.4	103.6	108.2	0.187	0.226	0.316	16.500	−0.1171	•••	100.4	•••	•••	0.231	•••
16.336	0.1590	104.4	105.3	110.2	0.158	0.192	0.267	16.497	−0.1207	99.2	100.7	105.5	0.206	0.230	0.320
16.239	0.1764	107.8	108.4	111.0	0.108	0.145	0.233	16.428	−0.1385	101.1	102.8	106.8	0.152	0.187	0.254
16.119	0.1936	•••	111.7	•••	•••	0.105	•••								

TABLE I (*continued*)

T (°C)	$\Delta\rho/\rho_c$	u (m/sec) 0.6	1	3	α_λ (Np) 0.6	1	3	T (°C)	$\Delta\rho/\rho_c$	u (m/sec) 0.6	1	3	α_λ (Np) 0.6	1	3
16.022	0.2051	113.9	114.1	115.1	0.0547	0.0887	0.169	16.302	−0.1651	...	105.5	...	...	0.127	...
15.891	0.2204	117.5	117.7	118.6	0.0376	0.0568	0.131	16.251	−0.1741	106.4	107.0	109.3	0.0730	0.102	0.156
15.881	0.2216	...	117.6	...	...	0.0628	...	16.119	−0.1920	...	109.1	...	...	0.0756	...
15.872	0.2226	118.2	118.2	119.3	...	0.0584	0.118	16.049	−0.2013	109.5	110.0	111.3	0.0479	0.0664	0.119
15.667	0.2424	...	122.5	123.1	...	0.0387	0.0797	15.881	−0.2169	...	111.7	...	...	0.0465	...
15.333	0.2694	...	128.4	128.8	...	0.0233	0.0608	15.682	−0.2363	114.4	114.4	114.9	0.0159	0.0280	0.0622
15.010	0.2922	...	133.9	134.6	...	0.0118	0.0421	15.476	−0.2531	116.1	115.9	116.2	0.0100	0.0200	0.0488
14.695	0.3117	...	139.3	139.1	...	0.0104	0.0241	15.243	−0.2716	117.7	117.8	117.8	0.0066	0.0148	0.0396
14.344	0.3315	...	144.4	144.7	...	0.0067	0.0224	15.010	−0.2842	...	118.6	...	...	0.0111	...
14.028	0.3508	...	148.5	148.6	...	0.0048	0.0163	14.809	−0.2989	120.0	119.9	119.9	0.0029	0.0085	0.0229
								14.695	−0.3030	...	120.0	...	...	0.0061	...
								14.566	−0.3122	121.2	121.2	121.1	...	0.0058	0.0176
								14.344	−0.3203	...	121.7	121.7	...	0.0037	...
								14.028	−0.3345	...	122.9	122.9	...	0.0032	0.0152

the same time, higher-order terms were retained in the expansions (18) and (19) for $A_0(T)$ and $\mu_0(T)$. Not all the parameters of the linear model were made adjustable in this least-squares analysis. The most reliable ones were assigned fixed values. The critical exponent β was set equal to 0.357 and T_c was given the value 289.793 K, in agreement with the results obtained from the analysis of our dielectric measurements in the coexisting phases (see Sec. III). A value of 1.843 for B could also be obtained from the dielectric data (since $B = K_2/2E_c$). From the values of $(\partial\rho/\partial\mu)_T$ along the critical isochore[20,21] we obtained $\Gamma = 0.0676$. From the slope of the critical isochore at the critical point HB obtained the value -6.02 for A_0',[19] and the same value has been used here. The power-series expansions for $A_0(T)$ and $\mu_0(T)$ were truncated after the fourth power in ϵ. This left us with the seven quantities α, A_0'', A_0''', A_0'''', μ_0'', μ_0''', and μ_0'''' as adjustable parameters. $A_0(T_c)$, $\mu_0(T_c)$, and $\mu_0'(T_c)$ were not retained since they did not enter into the physical quantities relevant for this analysis. The most important free parameter in the least-squares analysis was the critical exponent α. Since we assigned a fixed value to the critical exponent β, the values for the critical exponents γ and δ were determined from the value of α and the scaling relations

$$\gamma = 2 - \alpha - 2\beta , \tag{20}$$

$$\delta = (2 - \alpha - \beta)/\beta . \tag{21}$$

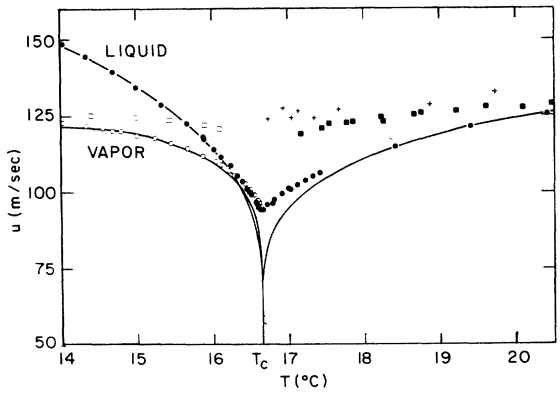

FIG. 6. Sound velocity in xenon in the saturated liquid and vapor phases and along the critical isochore for supercritical temperatures. The calculated thermodynamic values u (0) are represented by solid lines. The circles represent ultrasonic data at 1 MHz (open symbols for the saturated vapor, solid ones for the saturated liquid and for the critical isochore above T_c). Numerical values are given in Table I and in Ref. 8 (for the results along $\rho = \rho_c$). The squares are hypersonic data at ~300 MHz from Ref. 30 (solid symbols for $\rho = \rho_c$, open symbols for the saturated vapor phase). The pluses are hypersonic data at ~500 MHz along the critical isochore (Ref. 25).

TABLE II. 1-MHz sound velocity in both coexisting phases over the temperature range 5.5–14.4°C.

T (°C)	Sat. liquid u (m/sec)	Sat. vapor u (m/sec)
14.392	144.0	121.6
13.472	155.8	124.7
12.406	167.5	127.0
11.255	178.5	129.0
9.976	190.1	130.7
8.730	200.2	131.8
7.105	212.3	133.3
5.499	223.7	134.2

Also b^2 is then determined from the minimization condition Eq. (16). The parameter k is calculated from the relation

$$k = B(b^2 - 1)^{\beta}, \tag{22}$$

which can be obtained by comparing Eq. (10) with Eq. (8) for $\theta = 1$. From a comparison of Eq. (11) with the expression for the compressibility κ_T as a function of r and θ (see HB) for the case $\theta = 0$ one finds

$$a = k/\Gamma. \tag{23}$$

The parameters D and Γ/Γ' are given by Eqs. (14) and (15).

Table III summarizes the values of the parameters which gave the best fit to the experimental velocity data in the temperature range between 14 and 21°C. In Fig. 6 the calculated $u(0)$ values are compared with ultrasonic (1 MHz) and hypersonic values for $u(\omega)$ along the critical isochore and in both coexisting phases. Outside the dispersion region, the ultrasonic data are in very good agreement with the calculated $u(0)$ values. Deviations between an experimental velocity value used in the fit and the corresponding calculated value did not exceed 2%. It should be noted that the calculated $u(0)$ values in the saturated vapor just below T_c are larger than the corresponding values in the saturated liquid. The differences are probably not larger than the uncertainties in the calculated $u(0)$ values. Nevertheless this effect is definitely visible in the 1-MHz ultrasonic data over the same range of temperature. The reliability of our parameters for the linear model can be tested to some extent by a comparison with the recently obtained experimental results for $(\partial\rho/\partial\mu)_T$ along $\rho = \rho_c$ and along the coexistence curve.[20,21] The value of $\gamma = 1.207$ from our least-squares analysis is in very good agreement with the value 1.21 ± 0.03 obtained by Smith.[21] Our linear-model calculations gave a value of 4.03 for the ratio Γ/Γ'; 4.13 ± 0.2 is obtained experimentally. A direct calculation

TABLE III. Linear-model parameters for xenon.

Parameter	Value	Parameter	Value
T_c (K)	289.793	B	1.843
P_c (dyn cm^{-2})[a]	5.83×10^7	D	2.852
ρ_c (g cm^{-3})[a]	1.11	$A_0'(T_c)$[a]	−6.02
β	0.357	$A_0''(T_c)$	42.76
γ	1.207	$A_0'''(T_c)$	1.817×10^2
α	0.079	$A_0''''(T_c)$	-8.21×10^3
δ	4.38	$\mu_0''(T_c)$	−12.72
a	20.13	$\mu_0'''(T_c)$	−81.5
k	1.361	$\mu_0''''(T_c)$	-7.00×10^3
b^2	1.428	U_N(cm sec^{-1})[a,b]	7.280×10^3
Γ	0.0676	C_N (J mole^{-1} K^{-1})[a,b]	2.40
Γ/Γ'	4.030		

[a] Values taken from Ref. 16.

[b] $U_N = (P_c/\rho_c)^{1/2}$, $C_N = (P_c M/T_c\rho_c)\times10^{-7}$, where M is the molecular weight.

of $(\partial\rho/\partial\mu)_T$ is in very good agreement with the experimental results along both the critical isochore and the coexistence curve. Thus we have considerable confidence in the parameters listed in Table III, and we will attempt to use the linear model for calculating numerical values of the thermodynamic properties which occur in the expressions for the critical absorption and dispersion.

V. CRITICAL ABSORPTION AND DISPERSION

Detailed expressions for the critical absorption and dispersion of sound have been obtained by Kawasaki within the framework of mode-mode coupling theory.[22] Mistura[6,23] developed a modified version of Fixman's original approach involving energy transfer between sound waves and density fluctuations and obtained results identical to those presented by Kawasaki. In both the Kawasaki and the Mistura derivations, however, the velocity dispersion was assumed to be small. This is clearly a poor assumption close to the critical point of a pure fluid and we have been able to derive modified expressions for both the absorption and dispersion without making this assumption.[7]

One of the basic results of the theoretical predictions is that the critical absorption and dispersion depend primarily on a single reduced variable $\omega^* = \omega/\omega_D$, where $\omega = 2\pi f$ is the angular frequency and ω_D is a characteristic frequency for thermal diffusion. The frequency ω_D is defined by

$$\omega_D \equiv (2\Lambda/\rho C_p)\xi^{-2}, \tag{24}$$

where Λ is the thermal conductivity coefficient, C_p is the constant-pressure specific heat (i.e., heat capacity per gram), and ξ is the correlation length. The final expressions for the critical

absorption per wavelength and for the velocity dispersion are[7]

$$\alpha_\lambda(\text{crit}) = 2\pi u^2(\omega)\mathcal{A}I(\omega^*), \tag{25}$$

$$1 - u^2(0)u^{-2}(\omega) = 2u^2(0)\mathcal{A}J(\omega^*) \equiv \mathcal{B}J(\omega^*), \tag{26}$$

where

$$\mathcal{A} = \frac{k_B T^3}{2\pi^2\rho^3}(1 - \tfrac{1}{2}\eta)^2 \frac{1}{u^4(0)C_v^2}\left(\frac{\partial P}{\partial T}\right)_v^2 \kappa\left(\frac{\partial \kappa}{\partial T}\right)_S^2, \tag{27}$$

η is the critical exponent arising from the Fisher correction to the Ornstein-Zernike correlation function, and $\kappa \equiv \xi^{-1}$ is the inverse correlation length. $I(\omega^*)$ and $J(\omega^*)$ represent the following integrals:

$$I(\omega^*) = \int_0^\infty \frac{x^2\,dx}{(1+x^2)^2}\frac{\omega^* K(x)}{K^2(x) + \omega^{*2}} \tag{28}$$

$$J(\omega^*) = \int_0^\infty \frac{x^2\,dx}{(1+x^2)^2}\frac{\omega^{*2}}{K^2(x) + \omega^{*2}}, \tag{29}$$

where $K(x) = \frac{3}{4}\left[1 + x^2 + (x^3 - x^{-1})\arctan x\right]$ and $x \equiv q\xi$, with q being the wave number of the order-parameter (density) fluctuations. $\alpha_\lambda(\text{crit})$ is defined as as the difference between the measured total absorption per wavelength ($\alpha_{\lambda f} \equiv \alpha\lambda$) and the classical Navier-Stokes (NS) absorption given by[24]

$$\alpha_\lambda(\text{NS}) = \frac{\pi\omega}{\rho u^2(\omega)}\left[(\tfrac{4}{3}\eta_s + \zeta_0) + \Lambda(C_v^{-1} - C_p^{-1})\right], \tag{30}$$

where η_s is the shear viscosity, and ζ_0 is the normal "nonrelaxing" bulk viscosity which has approximately the same magnitude as the shear viscosity.[25,26] In order to carry out the analysis of the absorption results in terms of Eq. (25), the classical contribution was subtracted from the measured values given in Table I. It should, however, be pointed out that for ultrasonic frequencies the $\alpha_\lambda(\text{NS})$ contribution near the critical point was almost negligible compared to the attenuation arising from the relaxing bulk viscosity $\zeta(\omega)$. Only far away from the critical point does $\alpha_\lambda(\text{NS})$ make a significant contribution. For the data quoted in Table I the largest $\alpha_\lambda(\text{NS})$ contribution did not exceed 3% of the total measured value. In calculating $\alpha_\lambda(\text{NS})$ we made use of the thermal diffusivity $(\Lambda/\rho C_p)$ obtained by Lim, Swinney, Smith, and Benedek.[21,27,28] Values for the shear viscosity were derived from expressions obtained by Smith[21] which are based on recent measurements of Strumpf.[29] Values for C_p and C_v were calculated from the linear-model parametric equation of state, using the parameter values given in Table III.

From Eqs. (25)–(27) one can see that in order to establish a comparison between the theoretical predictions and our experimental results a variety of physical properties have to be known. Ideally one would like to use direct experimental results for all the quantities which occur in $\mathcal{A}$ and $\mathcal{B}$ in Eqs. (25)–(27). Since accurate experimental data are lacking, it would be desirable to use the linear-model parametric equation of state to calculate the prefactors $\mathcal{A}$ and $\mathcal{B}$. Calculation of the thermodynamic quantities in Eq. (27) presents no problem. However, it is shown in the Appendix that calculation of the term $\kappa(\partial\kappa/\partial T)_S^2$ is complicated, and the values of this term are sensitive to the values chosen for the linear-model parameters and the experimental value of the direct correlation length R. In view of the difficulties in obtaining reliable *a priori* values for the prefactors $\mathcal{A}$ and $\mathcal{B}$ in Eqs. (25) and (26), another less-general approach to the analysis of the critical absorption and dispersion will be adopted. As was done in Ref. 7, we shall evaluate the prefactor $\mathcal{A}$ from a least-squares fit of the experimental $\alpha_\lambda(\omega)u^{-2}(\omega)$ data to Eq. (25). The simple relation $\mathcal{B} = 2u^2(0)\mathcal{A}$ allows one to use the results of the attenuation fit to analyze the dispersion since linear-model values of $u(0)$ are known. This procedure will be followed here for a reanalysis of the critical isochore data and for the analysis of our new data along the coexistence curve and along supercritical isotherms. The resulting $\mathcal{A}$ variations will then be used to determine "acoustic" values of $\kappa(\partial\kappa/\partial T)_S^2$ along different paths,

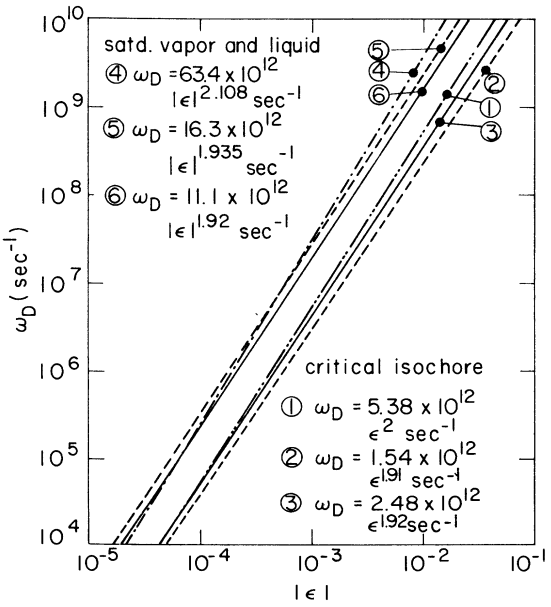

FIG. 7. Comparison of different power-law expressions for the characteristic frequency ω_D defined in Eq. (24). See Table IV and Sec. V A of the text for details.

TABLE IV. Various choices of ω_D and $\mathfrak{A}$ used in fitting α_λ data. Those parameters which were adjustable in the least-squares fitting procedure are shown underlined.

Path	Choice of ω_D	Curve in Fig. 7	$10^{-12}\omega_D$ (sec^{-1})	$10^6\mathfrak{A}$ (m^{-2} sec^2)
$\rho=\rho_c$	Ref. 7	1	$5.38\epsilon^{2}$	$\underline{7.3}\epsilon^{\underline{-0.22}}$
	Expt.	2	$1.54\epsilon^{1.91}$	$\underline{1.92}\epsilon^{\underline{-0.375}}$
	Eq. (43)[a]	3	$\underline{2.48}\epsilon^{1.92}$	$\underline{8.77}\epsilon^{-0.19}$
	Free[b]		$\underline{2.98}\epsilon^{\underline{1.905}}$	$\underline{7.03}\epsilon^{\underline{-0.22}}$
Coexistence curve	Expt.	4	$63.4\lvert\epsilon\rvert^{2.108}$	...
	Expt.	5	$16.3\lvert\epsilon\rvert^{1.935}$	$\underline{17.5}\lvert\epsilon\rvert^{\underline{-0.12}}L$
				$\underline{15.6}\lvert\epsilon\rvert^{\underline{-0.10}}V$
	Eq. (45)[a]	6	$\underline{11.1}\lvert\epsilon\rvert^{1.92}$	$\underline{8.33}(1+\underline{0.12}\theta)\lvert\epsilon\rvert^{-0.19}$
	Free[b]		$\underline{15.4}\lvert\epsilon\rvert^{\underline{2.00}}L$	$\underline{7.38}\lvert\epsilon\rvert^{\underline{-0.211}}L$
			$\underline{14.2}\lvert\epsilon\rvert^{\underline{1.99}}V$	$\underline{5.75}\lvert\epsilon\rvert^{\underline{-0.208}}V$

[a] These choices were the ones used in preparing the reduced attenuation and dispersion plots in Figs. 8 and 9.

[b] Four-parameter least-squares fit to the acoustic data without regard to experimental data on ω_D or scaling-law values of the exponents.

which can be compared with linear-model predictions.

A. Choice of ω_D

In order to carry out the above approach to the analysis of the acoustic data, it is necessary to establish a value for ω_D at each data point. For clarity and convenience, we shall discuss the choice of ω_D along all the different paths before proceeding to the actual analysis of α_λ for each separate path. As shown by Eq. (24), the direct determination of ω_D requires experimental data for both the thermal diffusivity and the correlation length. Such data are available only along the critical isochore and the coexistence curve. The resulting ω_D values are shown in curves 1, 2, 4, and 5 of Fig. 7 and are listed in Table IV. The ω_D variation along the path $\rho=\rho_c$ is well described by a power law of the type

$$\omega_D(\rho_c)=\omega_0\epsilon^{y}\,. \tag{31}$$

Curve 1 corresponds to $\omega_0=5.38\times10^{12}$ sec^{-1} and $y=2$, the choice made in Refs. 6 and 7 based on the best experimental data available at that time (see Ref. 6). This curve is given for comparison with the ω_D values represented by curve 2. These values are based on newer correlation lengths[20,21] and additional Rayleigh linewidths,[27] and the resulting parameters are $\omega_0=1.54\times10^{12}$ sec^{-1} and $y=1.91$. The ω_D variation along the coexistence curve can also be described fairly well by a simple power law,

$$\omega_D(\text{coex})=\omega_0'\lvert\epsilon\rvert^{y'}\,. \tag{32}$$

On the basis of the available data,[20,21,27,28] we have calculated ω_D and fit its variation in *both* coexisting phases over the range $3\times10^{-5}<\lvert\epsilon\rvert<10^{-3}$ with the parameters $\omega_0'=16.3\times10^{12}$ sec^{-1} and $y'=1.935$ (curve 5). However, these same data have been analyzed in the range $5\times10^{-4}<\lvert\epsilon\rvert<2\times10^{-2}$ to give rather different parameters, $\omega_0'=63.4\times10^{12}$ sec^{-1} and $y'=2.108$ (curve 4).[31] The reason for this difference will be discussed below in connection with our attempt to develop a parametric form for ω_D which can be used along arbitrary paths in ρ, T space.

If the thermal diffusivity $\Lambda/\rho C_p$ is written as the sum of a singular and a background part and the singular part $(\Lambda/\rho C_p)^s$ is replaced[22] by $k_BT/6\pi\eta^*\xi$, where η^* is the high-frequency shear viscosity coefficient, Eq. (24) can be written as

$$\omega_D=(k_BT/3\pi\eta^*)\xi^{-3}(1+\Lambda_b/\Lambda_s)\,. \tag{33}$$

Using Eqs. (A1) and (A7), this can be rewritten in the parametric form

$$\omega_D=\omega_0\chi^{3/2}(\theta)(1+\Lambda_b/\Lambda_s)r^{3\gamma/2}\,, \tag{34}$$

where ω_0 is independent of both r and θ. Unfortunately, Λ_b/Λ_s is not negligible (especially along the coexistence curve) and it varies with r. Thus ω_D(coex) does not follow a simple power law, and fits over different $\lvert\epsilon\rvert$ ranges will yield different exponents. However, close to the critical point

one can write as a good approximation

$$\omega_D \simeq \omega_0 \chi^{3/2}(\theta) r^y = 1.66\times 10^{12} \chi^{3/2}(\theta) r^{1.92} \text{ sec}^{-1}, \tag{35}$$

where a single exponent is used above and below T_c. The values of ω_0 and y in Eq. (35) were chosen to best represent the experimental ω_D data (curves 2 and 5 of Fig. 7), and indeed Eq. (35) describes these data as well as the two separate power laws given in Eqs. (31) and (32). Since $\chi(\theta)$ is an even function of θ, Eq. (35) is also consistent with the experimental fact that ω_D at a given $|\epsilon|$ value is the same in both coexisting liquid ($\theta = 1$) and vapor ($\theta = -1$). It should be noted that the adopted value of y is somewhat greater than $3\gamma/2 = 1.81$, which reflects the presence of the term $(1 + \Lambda_b/\Lambda_s)$ in Eq. (34).

It was hoped to use Eq. (35) to represent ω_D along various isotherms, where no experimental data for $\Lambda/\rho C_p$ or ξ are available. However, as will be discussed later, such a choice led to poor fits for our isothermal α_λ data. Thus a semiempirical form was assumed which retained the value 1.92 for the exponent y and the symmetry in θ but changed the character of the θ dependence:

$$\omega_D = \omega_0(1 + F\theta^2) r^y . \tag{36}$$

The two adjustable parameters ω_0 and F are no longer chosen to represent experimental ω_D values but are obtained from a simultaneous least-squares fit of our α_λ data along $\rho = \rho_c$ and various isotherms The value of the parameter F depends completely on the isothermal α_λ data, while ω_0 is largely determined by the α_λ data along ρ_c. As seen from Eq. (43a) and curve 3 of Fig. 7, the ω_D values predicted from this form along the critical isochore ($\theta = 0, r = \epsilon$) are larger by a factor of about 1.6 than those obtained from Eq. (35) or shown in curve 2 of Fig. 7. On the other hand, it should be noted in passing that the ω_D values obtained from Eq. (43a) along the coexistence curve [$\omega_D = 14.5\times 10^{12} |\epsilon|^{1.92}$] are almost the same as Eq. (35) or curve 5 of Fig. 7.

Finally, a different semiempirical form was tested for the coexistence curve:

$$\omega_D = \omega_1 |\epsilon|^y , \tag{37}$$

where the value 1.92 was again retained for the exponent y. This form looks like Eq. (32), but the adjustable parameter ω_1 is not chosen to fit experimental ω_D values but to achieve the best least-squares fit of our α_λ data in the liquid and vapor. As seen from Eq. (45a) and curve 6 of Fig. 7, the ω_D values along the coexistence curve predicted from this form are smaller by a factor of ~0.75 than those obtained from Eq. (35) or shown in curve 5 of Fig. 7.

B. Critical isochore

Let us begin with a comment on the extensive data obtained previously[8] at a mean filling density of $1.01\rho_c$. Comparison with the present isotherm data shows that gravity caused a small change in the local density with temperature during that run. Such density changes do not affect the megahertz velocities to any important extent since $u(\omega)$ is a very weak function of ρ near T_c. In the case of α_λ, however, the density dependence is stronger (see Fig. 3), and the critical attenuation data reported in Ref. 8 are low by ~15% near T_c. In terms of the analysis of these isochore data given in Ref. 7, the reduced sound dispersion is not changed at all and the reduced critical attenuation is the same up to $\omega^* \simeq 2$. The reduced ultrasonic attenuation in the range $2 \leq \omega^* \leq 500$ is larger than shown previously—a change which brings it into much better agreement with the reduced hypersonic attenuation at ~500 MHz. As far as fitting the critical absorption along $\rho = \rho_c$ with Eq. (25) is concerned, these changes are not important since $I(\omega^*)$ fails to represent α_λ values above $\omega^* \simeq 10$ anyway.[7]

In Ref. 7 the prefactor $\mathfrak{A}$ along the critical isochore was replaced by the simple power law

$$\mathfrak{A} = \mathfrak{A}_0 \epsilon^z , \tag{38}$$

and the parameters $\mathfrak{A}_0$ and z were determined by a least-squares fit of the experimental data to Eq. (25) using curve 1 of Fig. 7 for ω_D. The resulting values of $\mathfrak{A}_0$ and z were 7.3×10^{-6} m^{-2} sec^2 and -0.22.[7] It should be noted that Eq. (38) is consistent with the linear-model expression for $\kappa(\partial\kappa/\partial T)_\rho^2$ given in Eq. (A12) since it can be shown from Eqs. (1) and (27) that near the critical point

$$\mathfrak{A} \simeq \frac{k_B T}{2\pi\rho}\left(\frac{\partial P}{\partial T}\right)_v^{-2} \kappa \left(\frac{\partial \kappa}{\partial T}\right)_S^2 . \tag{39}$$

Along the path $\rho = \rho_c$, $(\partial P/\partial T)_v$ is essentially constant and $(\partial\kappa/\partial T)_S = (\partial\kappa/\partial T)_\rho$.

If Eq. (38) and the new "experimental" ω_D values given by curve 2 of Fig. 7 are used in a least-squares analysis of the $\alpha_\lambda(\omega)u^{-2}(\omega)$ data along the near-critical isochore, one obtains a fit to the data of about the same quality as that reported in Ref. 7. The values for $\mathfrak{A}_0$ and z are, however, significantly changed to 1.92×10^{-6} m^{-2} sec^2 and -0.375. From a four-parameter least-squares analysis in which ω_0, y, $\mathfrak{A}_0$, and z of Eqs. (31) and (38) are all treated as adjustable parameters, one obtains $\omega_0 = 2.98\times 10^{12}$ sec^{-1}, $y = 1.905$, $\mathfrak{A}_0 = 7.03 \times 10^{-6}$ m^{-2} sec^2, and $z = -0.22$. In the ϵ range of

interest, the values of $\mathfrak{A}(\epsilon)$ and $\omega_D(\epsilon)$ calculated from the latter fit agree very well with those calculated with the parameters reported in Ref. 7. All three fitting procedures described above and listed in Table IV give a good description of the $\alpha_\lambda(\omega)u^{-2}(\omega)$ data, indicating that the experimental uncertainties in this quantity leave some room for a range of ω_0 and y values if the values $\mathfrak{A}_0$ and z are simultaneously adjusted.

It is, however, helpful to consider the values of z, which equals $3\nu-2$ along the critical isochore. The value -0.375 gives $\nu=0.54$, whereas $z=-0.22$ gives $\nu=0.59$. Both these ν values are consistent with the value of 0.58 ± 0.05 reported from light scattering measurements,[20,21] but 0.59 is much closer to the linear-model value $\nu=\gamma/2=0.604$ [see Eqs. (A1) and (A7)]. Indeed, another fit to the critical-isochore data will be made with the exponent z fixed at its linear-model value $3\gamma/2-2=-0.19$. The details of this fitting procedure are given below in connection with the analysis of the isotherm data.

C. Isotherms

In order to analyze acoustic data along paths different from the critical isochore, it is natural to seek an extension of the power law, Eq. (38), in terms of a general linear-model parametric representation for Eq. (27). In particular, it would be attractive if one could write

$$\mathfrak{A}=\mathfrak{A}_1(\theta)r^z\,, \tag{40}$$

where $\mathfrak{A}_1(\theta)$ were a known function of θ. Unfortunately, such a simple form is not really valid in general. Since $(\partial\kappa/\partial T)_\rho$ is considerably larger than the second term in Eq. (A4), we find that

$$\kappa\left(\frac{\partial\kappa}{\partial T}\right)_s^2\simeq\kappa\left(\frac{\partial\kappa}{\partial T}\right)_\rho^2+2\kappa\left(\frac{\partial\kappa}{\partial T}\right)_\rho\left(\frac{\partial\kappa}{\partial\rho}\right)_T\frac{\rho^2C_v}{T(\partial P/\partial T)_v}\,. \tag{41}$$

The Appendix shows that the term $\kappa(\partial\kappa/\partial T)_\rho^2$ varies like $r^{3\gamma/2-2}$ times a complicated even function of θ [see Eq. (A11)], while the second term on the right-hand side of Eq. (41) varies like $r^{3\gamma/2-1-\beta-\alpha}$ times an odd function of θ.

For near-critical isotherms this last term in Eq. (41) is small, which is consistent with the experimental fact that our attenuation data along the isotherms are essentially symmetrical in density about ρ_c. Thus we have chosen the simple semiempirical form

$$\mathfrak{A}=\mathfrak{A}_0(1+G\theta^2)r^z\,, \tag{42}$$

where $\mathfrak{A}_0$ and G are adjustable parameters but z is held fixed at the value $3\gamma/2-2$.

In our initial efforts to analyze the α_λ data along various isotherms Eq. (35) was adopted for ω_D and the best least-squares values were obtained for the two parameters $\mathfrak{A}_0$ and G. These fits were poor and showed systematic deviations indicating that $\chi^{3/2}(\theta)$ gave too strong a θ dependence for ω_D along an isotherm. Therefore, the final analysis was carried out with a combination of Eq. (36) for ω_D and Eq. (42) for $\mathfrak{A}$. This approach involves four adjustable parameters ($\omega_0, F; \mathfrak{A}_0, G$) and two fixed exponents. In order to avoid too artificial a fitting procedure with so many parameters, the least-squares fit was made simultaneously for the α_λ data along all three supercritical isotherms and the critical isochore. The result of fitting all

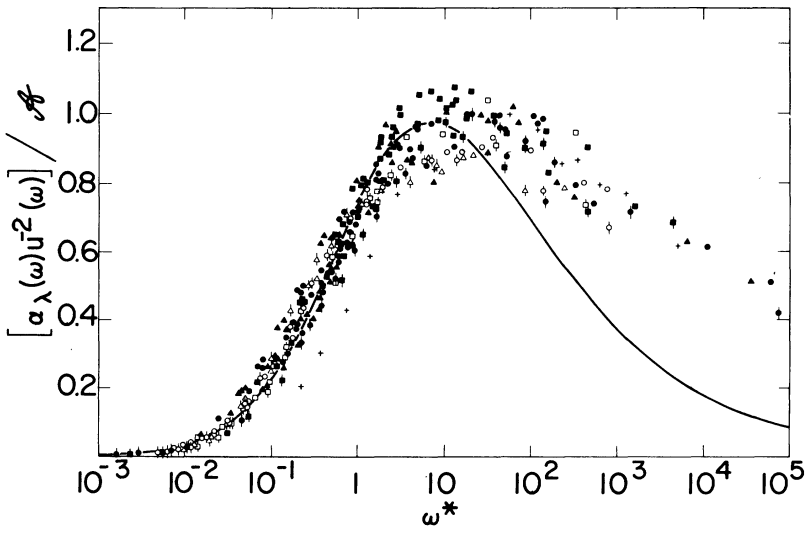

FIG. 8. Reduced critical sound absorption per wavelength as a function of ω^*. Ultrasonic data are shown at 0.6 MHz (triangles), 1 MHz (circles), and 3 MHz (squares). Solid symbols are used for the supercritical isotherms, and solid symbols with a vertical line for $\rho=\rho_c$. Open symbols are for the coexistence curve (with a vertical line for the liquid). The pluses are hypersonic data at ~500 MHz along the critical isochore (Ref. 25). The curve represents $2\pi I(\omega^*)$, where $I(\omega^*)$ is defined in Eq. (28).

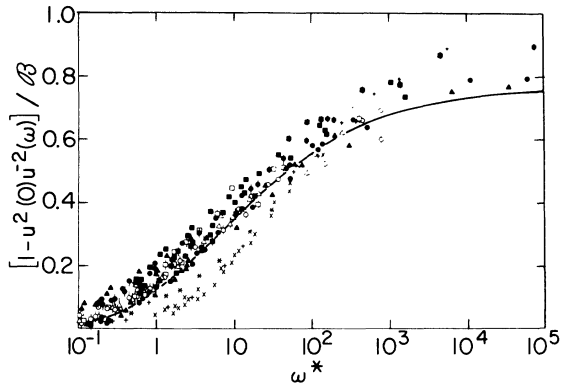

FIG. 9. Reduced sound dispersion as a function of ω^*. The symbols for data points are the same as those used in Fig. 8. Additional hypersonic data at ~300 MHz (Ref. 30) are indicated by crosses for $\rho=\rho_c$ and by stars for the saturated vapor. The line represents the integral $J(\omega^*)$ defined in Eq. (29).

such data where $\omega^* \leq 10$ gave

$$\omega_D = 2.48\times10^{12}(1+0.15\theta^2)r^{1.92}\ \text{sec}^{-1}, \qquad (43a)$$

$$\mathcal{G} = 8.77\times10^{-6}(1+0.10\theta^2)r^{-0.19}\ \text{m}^{-2}\,\text{sec}^2 \qquad (43b)$$

The reduced critical absorption and dispersion obtained with the use of Eqs. (43) are shown in Figs. 8 and 9 for the isotherms and for the critical isochore. For the latter path, it should be noted that this fit depends on only two adjustable parameters and compares very closely to those discussed in Sec. V B (see Table IV).

Although no acoustic data were directly measured along the critical isotherm ($T_c = 16.643$°C) it is possible to infer the behavior along that line from an interpolation involving all our available data (including one subcritical isotherm). As shown in Fig. 5, α_λ and u values at megahertz frequencies do not vary too rapidly with temperature near the critical point. Thus it turns out that interpolated $\alpha_\lambda(\omega)$ and $u(\omega)$ values along the critical isotherm are almost exactly the same as the values tabulated for the 16.669°C isotherm. A calculation of the density dependence of properties along the critical isotherm ($\epsilon = 0$, $\theta = \pm 1/b$) can be readily carried out since Eq. (8) gives $r = (b/k)^{1/\beta}|\Delta|^{1/\beta}$ in this case. For noncritical isotherms, r is a function of both ϵ and Δ; thus no simple power law in terms of Δ is possible.

D. Coexistence curve

As a first procedure, we shall analyze our α_λ data in the coexisting liquid and vapor by using the "experimental" ω_D values given by curve 5 of Fig. 7 and assuming that $\mathcal{G}$ has a form like Eq. (40) with two adjustable parameters chosen separately for each phase. A least-squares fit of all the $\alpha_\lambda(\omega)u^{-2}(\omega)$ data for which $\omega^* \leq 10$ gave $\mathcal{G} = 17.5\times10^{-6}|\epsilon|^{-0.12}$ m^{-2} sec^2 for the liquid phase and $15.6\times10^{-6}|\epsilon|^{-0.10}$ m^{-2} sec^2 for the vapor phase. However, these fits were not as good as the one which was obtained for $\rho=\rho_c$ using experimental ω_D values. It should also be noted from Table IV that the use of the best available experimental ω_D values yields quite different values for the exponent z above and below T_c(−0.375 compared with approximately −0.11). In spite of the complicated linear-model form for $\mathcal{G}$ discussed in connection with Eq. (41), one would expect essentially the same dominant divergence in $\mathcal{G}$ along the critical isochore and the coexistence curve.

A much better fit to the α_λ(coex) data can be achieved with a four-parameter least-squares analysis in which the coefficients and exponents in Eqs. (32) and (40) are all treated as free parameters and allowed to assume different values in each phase. The resulting values of the parameters for ω_D and $\mathcal{G}$ are given in Table IV. The values of ω_D calculated from these parameters are almost the same for each phase but differ from the experimental results by a factor of about 1.6 over the $|\epsilon|$ range of interest (the ϵ dependence being roughly the same). It should be noted that the value of z is independent of the phase and is almost equal to the value obtained from an identical type of fit for the data along the critical isochore.

The fact that our coexistence data are completely compatible with a single ω_D variation for both phases and a single exponent describing the divergence of the prefactor $\mathcal{G}$ has led us to a final analysis based on the use of Eq. (37) for ω_D and the form

$$\mathcal{G} = \mathcal{G}_1(1+H\theta)|\epsilon|^z, \qquad (44)$$

where $\mathcal{G}_1$ and H are adjustable parameters but z is held fixed at the linear-model value of −0.19.[32] Equation (44) is a convenient way of representing the asymmetry of our data along the liquid ($\theta = 1$) and vapor ($\theta = -1$) sides of the coexistence curve; see Sec. V E for a more detailed discussion of $\mathcal{G}$(coex) in terms of the linear model. The result of fitting all our coexistence-curve data where $\omega^* \leq 10$ gave

$$\omega_D = 11.1\times10^{12}|\epsilon|^{1.92}\ \text{sec}^{-1}, \qquad (45a)$$

$$\mathcal{G} = 8.33\times10^{-6}(1+0.12\theta)|\epsilon|^{-0.19}\ \text{m}^{-2}\,\text{sec}^2. \qquad (45b)$$

The reduced critical absorption and dispersion obtained in both coexisting phases with the use of Eqs. (45) are shown in Figs. 8 and 9.

E. Discussion of fits

We now wish to make some general comments on the reduced absorption and dispersion variations displayed in Figs. 8 and 9 and to compare the prefactors $\mathfrak{A}$ obtained from our least-squares fits with those expected on the basis of the linear-model parametric equation of state.

It can be seen from Fig. 8 that all of our ultrasonic data along different paths can be represented very well by Eq. (25) up to $\omega^* \simeq 10$. Furthermore, reduced absorptions at larger ω^* values are quite consistent with each other in spite of lying systematically above the theoretical curve. Indeed, such deviations from Eq. (25) are expected[22] and can be ascribed to the breakdown at large ω^* of the Ornstein-Zernike form for the fluctuations.[6] Figure 9 shows that the reduced dispersion is quite well represented by Eq. (26). Note that the quantity $\mathfrak{B}$ is not adjusted to fit the observed dispersion but is obtained from $\mathfrak{B} = 2u^2(0)\mathfrak{A}$. Thus we can conclude that the observed ultrasonic absorption and dispersion along each path are compatible with each other and with the predictions of Kawasaki-Mistura theory.

Also shown in Figs. 8 and 9 are limited hypersonic data along $\rho = \rho_c$ and the vapor side of the coexistence curve. Equations (43) were used to reduce the direct experimental data along the critical isochore, and Eqs. (45) were used for the saturated vapor. The Brillouin points at small ω^* values lie below the ultrasonic results and below the theoretical curves. However, the values of $\Delta T = T - T_c$ corresponding to these particular hypersonic points are much larger than the ΔT values for any of our ultrasonic points. Thus most of the apparent discrepancy may be due to the use of expressions for ω_D and $\mathfrak{A}$ which are not valid far from T_c. Indeed, a recent small-angle Brillouin study[33] of saturated xenon vapor indicates good agreement between theory and experiment for frequencies between 2.4 and 24 MHz (corresponding to ΔT values in the range $-0.2°$ to $-7°$).

The conclusion that the Kawasaki-Mistura theory is a valid representation of our ultrasonic data depends not only on the quality of the fits shown in Figs. 8 and 9 but also on the reasonableness of the ω_D and $\mathfrak{A}$ values used in fitting the data. The ω_D variations have been shown in Fig. 7 and discussed previously. The $\mathfrak{A}$ values will be discussed here in terms of the behavior of $\kappa(\partial\kappa/\partial T)_S^2$. All the other quantities in Eq. (27) can be calculated very reliably from the linear-model parameters in Table III. This is indicated by Eq. (39) and the fact that linear-model values of $(\partial P/\partial T)_v$ agree well with values calculated directly from experimental data on the equation of state.[34]

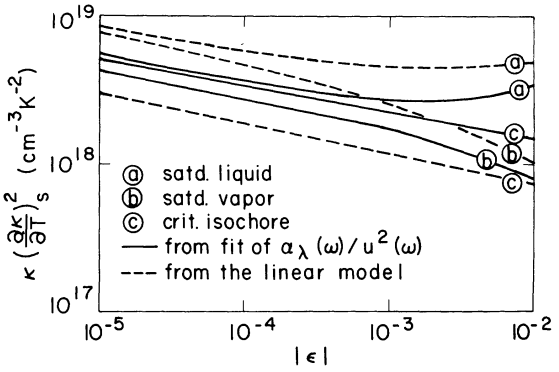

FIG. 10. Variation of $\kappa(\partial\kappa/\partial T)_S^2$ along the critical isochore and coexistence curve. Solid lines show the values obtained from a least-squares fit of the critical absorption data; dashed lines were calculated from the linear model using the parameters given in Table III.

Figure 10 shows the $\kappa(\partial\kappa/\partial T)_S^2$ variations obtained from the fit to our $\alpha_\lambda(\omega)u^{-2}(\omega)$ data along the critical isochore and along the coexistence curve. Equation (43a) was used for ω_D in the former case and Eq. (45a) in the latter. It is clear from this figure that although $\kappa(\partial\kappa/\partial T)_S^2$ follows a simple power law along the critical isochore, it does not do so along the coexistence curve. Also shown in Fig. 10 are the corresponding $\kappa(\partial\kappa/\partial T)_S^2$ values calculated from the linear model (see the Appendix). Over all there is good agreement in the temperature variations (especially the asymmetry on the coexistence curve) shown in these two sets of results. However, the distinct difference in magnitude between the linear-model values for $\rho = \rho_c$ and the coexistence curve is not present in the least-squares "acoustic" values. This splitting in the calculated $\kappa(\partial\kappa/\partial T)^2$ values is quite sensitive to the linear-model parameters (see the Appendix), but rather unlikely parameters would be required to eliminate the difference. On the other hand, the disagreement between the linear model and acoustic values of $\kappa(\partial\kappa/\partial T)^2$ along the critical isochore, which amounts to a roughly constant factor of 1.8, could easily be eliminated if the value of R_c in Eq. (A12) were reduced by ~20%.

In view of the difficulties in carrying out linear-model calculations of $\kappa(\partial\kappa/\partial T)_S^2$ and the existing uncertainties in the experimental data needed to determine ω_D and $\mathfrak{A}$ directly, we consider the analysis presented here to indicate good agreement between Kawasaki-Mistura theory and our acoustic data along many paths. Even better agreement, involving no adjustable parameters, is claimed in Ref. 33. However, that agreement was achieved only with data at low values of ω^* along a single path (saturated vapor). More extensive and more

precise experimental information on the correlation length and the thermal diffusivity will be needed before a more rigorous analysis of the acoustic properties will be possible.[35]

VI. SUMMARY

In this paper we have presented detailed experimental results for the sound absorption and velocity near the critical point of xenon. The data were obtained as a function of the density by simultaneously measuring the dielectric constant at the same level in the fluid as that at which ultrasonic data were taken. Results were obtained for three frequencies (0.6, 1, and 3 MHz) along both sides of the coexistence curve and along four isotherms. The data for the dielectric constants in the coexisting phases yielded a value of 0.357 ± 0.002 for the critical exponent β. This value of β agrees very well with the recently obtained values of 0.3574 ± 0.0027 for argon and 0.3571 ± 0.0008 for krypton.[36] Numerical values for the thermodynamic sound velocity $u(0)$ and for other thermodynamic quantities needed in the analysis of $\alpha_\lambda(\omega)$ and $u(\omega)$ were calculated with the linear-model parametric equation of state. A linear-model calculation of the prefactors $\mathfrak{A}$ and $\mathfrak{B}$ in Eqs. (25) and (26) was, unfortunately, not sufficiently reliable for the analysis of the acoustic absorption and dispersion. An alternative least-squares fitting procedure for the critical absorption and dispersion showed that these quantities can be well described in terms of the Kawasaki-Mistura theory.

ACKNOWLEDGMENTS

We greatly appreciate helpful discussions with Dr. D. Eden, Professor H. L. Swinney, and Professor H. Z. Cummins.

APPENDIX: LINEAR-MODEL EXPRESSIONS FOR THE INVERSE CORRELATION LENGTH AND ITS TEMPERATURE DERIVATIVES

To calculate the terms involving the inverse correlation length $\kappa \equiv \xi^{-1}$ in Eq. (27) from the linear model, one must assume the validity of the Ornstein-Zernike relation

$$\frac{\xi^2}{R^2} = \frac{\kappa_T}{\kappa_I} = \frac{k_B T}{m\rho}\left(\frac{\partial \rho}{\partial \mu}\right)_T, \tag{A1}$$

where $\kappa_T = (\partial\rho/\partial\mu)_T/\rho^2$ is the isothermal compressibility, μ is the chemical potential per gram, m the mass of a molecule, κ_I is the compressibility of an ideal gas at the number density ρ_N (i.e., $\kappa_I^{-1} = k_B T \rho_N$), and R is the direct correlation length which is assumed to play the role of an average interparticle distance.

From the preceding it follows that κ can be considered as a quantity depending explicitly on ρ and T for which the following relation holds:

$$\left(\frac{\partial \kappa}{\partial T}\right)_S = \left(\frac{\partial \kappa}{\partial T}\right)_\rho + \left(\frac{\partial \kappa}{\partial \rho}\right)_T \left(\frac{\partial \rho}{\partial T}\right)_S . \tag{A2}$$

Since

$$\left(\frac{\partial T}{\partial \rho}\right)_S = \frac{T}{\rho^2}\frac{(\partial P/\partial T)_\rho}{C_v} , \tag{A3}$$

one obtains immediately

$$\left(\frac{\partial \kappa}{\partial T}\right)_S = \left(\frac{\partial \kappa}{\partial T}\right)_\rho + \left(\frac{\partial \kappa}{\partial \rho}\right)_T \frac{\rho^2 C_v}{T(\partial P/\partial T)_\rho} . \tag{A4}$$

Linear-model expressions for the quantities C_v and $(\partial P/\partial T)_\rho$ are given in dimensionless units by Eqs. (A8) and (A21) of Hohenberg and Barmatz.[16,19]

Differentiation of Eq. (A1) leads to the following expressions:

$$\left(\frac{\partial \kappa}{\partial T}\right)_\rho = \frac{\kappa}{2}\frac{1}{T_c}\left\{\left(\frac{\partial \mu}{\partial \rho}\right)_T^{-1}\left[\frac{\partial}{\partial T}\left(\frac{\partial \mu}{\partial \rho}\right)_T\right]_\rho - \frac{1}{T} - \frac{2}{R}\left(\frac{\partial R}{\partial T}\right)_\rho\right\}, \tag{A5}$$

$$\left(\frac{\partial \kappa}{\partial \rho}\right)_T = \frac{\kappa}{2}\frac{1}{\rho_c}\left\{\left(\frac{\partial \mu}{\partial \rho}\right)_T^{-1}\left(\frac{\partial^2 \mu}{\partial \rho^2}\right)_T + \frac{1}{\rho} - \frac{2}{R}\left(\frac{\partial R}{\partial \rho}\right)_T\right\}, \tag{A6}$$

where the quantities in curled brackets are all in dimensionless units. Use is made now of the linear-model expression[16]

$$\left(\frac{\partial \mu}{\partial \rho}\right)_T = ak^{-1}\gamma^\gamma \chi(\theta) , \tag{A7}$$

where $\chi(\theta)$ is an even function of θ given in Eq. (A20) of HB. After some lengthy but straightforward manipulations, we obtain

$$\left(\frac{\partial \mu}{\partial \rho}\right)_T^{-1}\left[\frac{\partial}{\partial T}\left(\frac{\partial \mu}{\partial \rho}\right)_T\right]_\rho = \frac{1}{\gamma}\frac{\gamma - \beta\theta\chi^{-1}(\theta)\,\partial\chi(\theta)/\partial\theta}{1 + (2\beta - 1)b^2\theta^2} , \tag{A8}$$

$$\left(\frac{\partial \mu}{\partial \rho}\right)_T^{-1}\left(\frac{\partial^2 \mu}{\partial \rho^2}\right)_T = \frac{1}{k\gamma^\beta}\frac{2\gamma b^2\theta + (1 - b^2\theta^2)\chi^{-1}(\theta)\,\partial\chi(\theta)/\partial\theta}{1 + (2\beta - 1)b^2\theta^2} . \tag{A9}$$

In order to calculate $\kappa(\partial\kappa/\partial T)_S^2$ from the above equations, it is necessary to know the direct correlation length R as a function of density and temperature. Smith, Giglio, and Benedek have shown that R is independent of temperature and depends only

weakly on density[20,21] near the critical point of xenon. Smith[21] proposed the following expression:

$$R = R_c(\rho/\rho_c)^{1/2} = 4.9(\rho/\rho_c)^{1/2}\ \text{Å}, \tag{A10}$$

which is based on the notion that at any given $|\epsilon|$ value the ratio of the experimental κ value for $\rho = \rho_c$ above T_c to that on the coexistence curve was equal to the corresponding ratio of $(\partial\mu/\partial\rho)_T^{1/2}$ values. Unfortunately, the experimental R values below T_c given in Ref. 21 do not completely substantiate the notion of a square-root density dependence. On the other hand, support for the direct correlation length being proportional to $\rho^{1/2}$ has recently been obtained from small-angle x-ray scattering measurements.[37] A happy consequence of the choice of Eq. (A10) for R is the fact that the last two terms in Eq. (A6) then cancel each other.

Using the linear-model parameters given in Table III and Eq. (A10) for R, we calculated values of $\kappa(\partial\kappa/\partial T)_S^2$ from the appropriate combination of Eqs. (A1)–(A9). These calculated values along the critical isochore and along both sides of the coexistence curve are shown in Fig. 10 and are discussed in Sec. V E in comparison with the empirical values obtained from fitting our acoustic data. It can be seen from that discussion that the linear-model values appear to be low along $\rho = \rho_c$ and high along the coexistence curve. The major source of uncertainty in the calculated $\kappa(\partial\kappa/\partial T)_S^2$ values must arise from $(\partial\kappa/\partial T)_\rho$ since the second term in Eq. (A4) is exactly zero for $\rho = \rho_c$ and goes to zero as $r \to 0$ along the coexistence curve. Since $(\partial R/\partial T)_\rho = 0$ and the term $1/T$ in Eq. (A5) is small enough to be neglected, one can easily obtain

$$\kappa\left(\frac{\partial\kappa}{\partial T}\right)_\rho^2 = \frac{1}{4T_c^2}\left(\frac{mP_c}{\rho_c k_B T}\right)^{3/2} \times \left(\frac{a}{R_c^2 k}\right)^{3/2} \chi^{3/2}(\theta) f^2(\theta) r^{3\gamma/2-2}, \tag{A11}$$

where $f(\theta)/r$ represents the right-hand side of Eq. (A8). For the critical isochore Eq. (A11) reduces to

$$\kappa\left(\frac{\partial\kappa}{\partial T}\right)_{\rho_c}^2 = \frac{1}{4T_c^2}\left(\frac{mP_c}{\rho_c k_B T}\right)^{3/2} (R_c^2\Gamma)^{-3/2}\gamma^2\epsilon^{3\gamma/2-2}. \tag{A12}$$

In both Eqs. (A11) and (A12) all the quantities are expressed in normal units; note, however, that the linear-model parameter $\Gamma = a/k$ is dimensionless.

Since our value of γ is quite accurate and in agreement with the experimental value found for this parameter,[21] one may conclude that the uncertainty in $\kappa(\partial\kappa/\partial T)_{\rho_c}^2$ must arise from the term $(R_c^2\Gamma)^{-3/2}$. Using the values of R_c and Γ reported by Smith, Giglio, and Benedek,[20,21] we obtain from Eq. (A12) $\kappa(\partial\kappa/\partial T)_{\rho_c}^2 = 3.39\times10^{17}\epsilon^{-0.19}\ \text{cm}^{-3}\,\text{K}^{-2}$, which is represented by the dashed curve c in Fig. 10. If the reported experimental uncertainties in R_c and Γ are taken into account and lower limits for these quantities are used, the calculated values of $\kappa(\partial\kappa/\partial T)_{\rho_c}^2$ can be increased by a factor of 1.4. However, this is only about half the discrepancy shown in Fig. 10.[38]

It can also be shown that the θ-dependent terms in Eq. (A11) are quite sensitive to the values of the linear-model parameters. Thus the ratio of $\kappa(\partial\kappa/\partial T)_\rho^2$ along the coexistence curve to that along the critical isochore at a given $|\epsilon|$ value is 2.8 for our parameters, 3.7 for the HB parameters, and could be as low as 2.0 for a rather arbitrary choice of parameters satisfying Eqs. (16), (20), and (21).

In view of the above, it does not seem possible to calculate linear-model values for $\kappa(\partial\kappa/\partial T)_S^2$ with an accuracy in their magnitude of better than about a factor of 2. However, the dependence on ϵ (or r) seems to be much better defined, and this will be useful in carrying out the semiempirical analysis of the acoustic data in Sec. V.

*Research supported in part by the National Science Foundation.

†On leave of absence 1971–72 from the Molecular Physics Section, Department of Physics, University of Leuven, Leuven, Belgium. Supported in part by NATO.

[1]C. W. Garland, in *Physical Acoustics*, edited by W. P. Mason and R. N. Thurnston (Academic, New York, 1970), Vol. 7, Chap. 2.

[2]D. Sette, in *Proceedings of the Enrico Fermi International School of Physics: Critical Phenomena*, edited by M. S. Green (Academic, New York, 1971), p. 508.

[3]J. Thoen, E. Vangeel, and W. Van Dael, Physica 52, 205 (1971); G. T. Feke, K. Fritsch, and E. F. Carome, Phys. Rev. Lett. 23, 1282 (1969).

[4]J. L. Kline and E. F. Carome, J. Chem. Phys. 58, 4962 (1973).

[5]C. W. Garland and R. Williams, following article, Phys. Rev. A 10, 1328 (1974).

[6]C. W. Garland, D. Eden, and L. Mistura, Phys. Rev. Lett. 25, 1161 (1970).

[7]D. Eden, C. W. Garland, and J. Thoen, Phys. Rev. Lett. 28, 726 (1972).

[8]P. E. Mueller, D. Eden, C. W. Garland, and R. C. Williamson, Phys. Rev. A 6, 2272 (1972).

[9]R. C. Williamson and D. Eden, J. Acoust. Soc. Am. 47, 1278 (1970).

[10]P. E. Mueller, Ph.D. thesis (Chemistry Department, Massachusetts Institute of Technology, 1969) (un-

published).
[11]J. A. Chapman, P. C. Finnimore, and B. L. Smith, Phys. Rev. Lett. 21, 1306 (1968).
[12]A. Cops, M. Caubergh, and W. Van Dael, *Proceedings III International Cryogenic Engineering Conference* (Iliff Science and Technology, Guildford, England, 1970).
[13]P. Schofield, J. D. Litster, and J. T. Ho, Phys. Rev. Lett. 23, 1098 (1969); see also C. Huang and J. T. Ho, Phys. Rev. A 7, 1304 (1973).
[14]P. Schofield, Phys. Rev. Lett. 22, 606 (1969).
[15]B. D. Josephson, J. Phys. C 2, 1113 (1969).
[16]P. Hohenberg and M. Barmatz, Phys. Rev. A 6, 289 (1972).
[17]M. E. Fisher, in *Proceedings of the Enrico Fermi International School of Physics: Critical Phenomena*, edited by M. S. Green (Academic, New York, 1971), p. 1.
[18]The symbols for the different thermodynamic properties are also identical except that we use ϵ instead of t for the reduced temperature.
[19]It should be noted that in Ref. 16 the values quoted in Table I for A_0' should have a minus sign and the subscript s should be added to the entropy S in Eq. (A21).
[20]I. Smith, M. Giglio, and G. B. Benedek, Phys. Rev. Lett. 27, 1556 (1971).
[21]I. W. Smith, Ph.D. thesis (Physics Department, Massachusetts Institute of Technology, 1972) (unpublished).
[22]K. Kawasaki, Phys. Rev. A 1, 1790 (1970).
[23]L. Mistura, in *Proceedings of the Enrico Fermi International School of Physics: Critical Phenomena*, edited by M. S. Green (Academic, New York, 1971), p. 563.
[24]K. F. Herzfeld and T. A. Litovitz, *Absorption and Dispersion of Ultrasonic Waves* (Academic, New York, 1959).
[25]D. S. Cannell and G. B. Benedek, Phys. Rev. Lett. 25, 1157 (1970); D. S. Cannell, Ph.D. thesis (Massachusetts Institute of Technology, 1970) (unpublished).
[26]P. Gray and S. A. Rice, J. Chem. Phys. 41, 3689 (1964).
[27]T. K. Lim, H. L. Swinney, I. W. Smith, and G. B. Benedek, Opt. Commun. 7, 18 (1973).
[28]T. K. Lim and H. L. Swinney (private communication).
[29]H. J. Strumpf, Ph.D. thesis (California Institute of Technology, 1972) (unpublished); H. J. Strumpf, A. F. Collins, and C. J. Pings, J. Chem. Phys. 60, 3109 (1974).
[30]H. Z. Cummins and H. L. Swinney, Phys. Rev. Lett. 25, 1165 (1970); H. Z. Cummins (private communication).
[31]D. Eden (private communication).
[32]The use of the subscript 1 is to remind one that Eq. (44) is not intended to reduce to Eq. (38) when θ is set equal to zero. Since $\epsilon = (1-b^2)r$ along the coexistence curve, the linear model would predict $\mathfrak{A}_0 = \mathfrak{A}_1(1-b^2)^x$ even if $\mathfrak{A}_1$ had no implicit θ dependence.
[33]D. Eden and H. L. Swinney, Opt. Commun. 10, 191 (1974).
[34]F. Theeuwes and R. J. Bearman, J. Chem. Thermodynamics 2, 501 (1970); D. H. Garside, H. V. Mølgaard, and B. L. Smith, J. Phys. B 1, 449 (1968).
[35]It should be noted that a recent ultrasonic investigation [D. Roe, B. Wallace, and H. Meyer, Phys. Rev. A (to be published)] of He^4 along $\rho = \rho_c$ has been analyzed in terms of Kawasaki-Mistura theory with good internal consistency but with fairly large differences between the acoustic values of ω_0 and $\mathfrak{A}_0$ and the values predicted from critical light scattering experiments.
[36]C. J. Pings, J. Chem. Phys. (to be published).
[37]J. V. Sengers, AIP Conf. Proc. 11, 229 (1973), and references therein.
[38]It should be noted that the linear-model parameters of HB give $\kappa(\partial\kappa/\partial T)^2_{\rho_c} = 4.05\times10^{17}\,\epsilon^{-0.13}$ cm^{-3}K^{-2}, which predicts values even lower (by a factor of 1.4 at $\epsilon = 10^{-4}$) than dashed curve c in Fig. 10. Direct differentiation of the power-law fit $\xi = 3.0\,\epsilon^{-0.58}$ Å for the experimental correlation length along the critical isochore (Ref. 20) gives $\kappa(\partial\kappa/\partial T)^2_{\rho_c} = 1.48\times10^{17}\,\epsilon^{-0.26}$ cm^{-3}K^{-2}, with fairly wide limits of error due to the reported uncertainty of ±0.05 in ν. The values calculated from this expression agree well with dashed curve c in Fig. 10 at $\epsilon = 10^{-5}$ but lie below it by a factor of 1.5 at $\epsilon = 10^{-2}$.